PAPER

Development of high-silica fly ash-based adsorbents for efficient dye removal from wastewater: a comparative study of MSAM and SDS/FA

Xuying Guo, [ID] *[ab] Xiaoyue Zhang,[b] Xinle Gao,[c] Yanrong Dong,[b] Zilong Zhao[c] and Honglei Fu[b]

Solid waste fly ash is challenged by accumulation, storage, low comprehensive utilization, insufficient high-value use technologies, and environmental and ecological risks. Owing to its high silicon content and superior adsorption capability, two novel adsorbents—mesoporous silicon aluminum material (MSAM) and sodium dodecyl sulfate modified fly ash (SDS/FA)—were prepared using ultrasonic-assisted, alkali fusion–hydrothermal, and surface modification methods. Their ability to enhance the adsorption of dyes (MB, MV) on high-silica fly ash through various modification strategies was explored. The effects of the alkali-to-ash ratio, ultrasonic time, hydrothermal time, and hydrothermal temperature on MSAM adsorption were evaluated, and the optimal preparation conditions were determined using Box–Behnken response surface methodology. Likewise, the impact of particle size, SDS dosage, ultrasonic time, and oscillation time on the SDS/FA system was analyzed, and optimal conditions were established. XRD, SEM, FTIR, and BET were used for characterization. Dynamic column experiments assessed the performance of SDS/FA in removing MB and MV from dye wastewater. Results showed that: (1) MSM and SDS/FA optimal preparation conditions were determined, with MSAM (alkali-to-ash ratio 1.2 : 1, ultrasonic 20 min, hydrothermal 8 h, 100 °C) achieving 94.70% and 80.05% removal for MB and MV, respectively; SDS/FA (0.25–0.38 mm, 3 g SDS, 20 min ultrasound, 8 h oscillation) achieved 85.33% and 95.38%. Characterization revealed significantly enhanced surface area and active sites. (2) Dynamic experiments demonstrated that SDS/FA columns increased MB and MV removal by 34.41% and 37.92% compared to high-silica fly ash, with stable effluent pH over time. The static adsorption of MSAM supports its application in dye wastewater treatment, and the structure–property relationship provides a new pathway for the high-value use of fly ash.

[a]*College of Science, Liaoning Technical University, Fuxin 123000, Liaoning, China. E-mail: guoxuying@lntu.edu.cn; Tel: +86-24-13941834560*

[b]*College of Civil Engineering, Liaoning Technical University, Fuxin 123000, Liaoning, China*

[c]*College of Mining, Liaoning Technical University, Fuxin 123000, Liaoning, China*

1 Introduction

With the rapid development of industries such as textiles, dyeing, and papermaking, dye wastewater has become a major component of industrial effluents.[1,2] It is estimated that more than 700 000 tons of dye wastewater are discharged globally each year, with approximately 10% to 15% of dyes entering water bodies during production and use, resulting in severe environmental pollution.[3] Dye wastewater typically contains high concentrations of organic dyes, among which methylene blue (MB) and methyl violet (MV) are notable for their high chromaticity, toxicity, and resistance to degradation.[4] If

discharged without effective treatment, such wastewater not only reduces the transparency of water bodies and disrupts aquatic ecosystems, but may also bioaccumulate through the food chain, posing risks to human health.[5] Currently, the primary methods for treating dye wastewater include chemical precipitation,[6] photocatalysis,[7] biological treatment,[8] and adsorption.[9] Among these, adsorption has received significant attention due to its operational simplicity, controllable cost, and strong adaptability. Adsorbent materials are crucial to the application of adsorption technology. However, conventional adsorbents such as ion exchange resins,[10] biochar,[11] activated carbon,[12] and graphene[13] each have their limitations. Ion exchange resins face high regeneration costs; commercial activated carbon and graphene, although possessing high adsorption capacities, require complex preparation processes involving high-temperature activation or chemical vapor deposition; and low-cost biochar often suffers from poor selectivity and slow adsorption rates. These techno-economic challenges

have prompted the development of novel adsorbents derived from industrial solid waste. By preparing composite materials from high-silica fly ash, a type of solid waste, it is possible to combine the cost advantages of biochar with the high-silica characteristics of fly ash, thereby enabling the efficient adsorption of dye ions.

Fly ash is a solid waste generated during coal combustion in thermal power plants.[14] In China, the annual production of fly ash exceeds 600 million tons, with a cumulative stockpile surpassing 3 billion tons.[15] Currently, the main applications of fly ash are in cement production[16] and road construction,[17] which are increasingly insufficient to accommodate the ever-growing quantities of this material. Thus, it is imperative to explore higher-value, more sustainable resource utilization pathways. In recent years, extensive research efforts have focused on employing fly ash as an adsorbent for environmental remediation, owing to its abundance of silicon and aluminum and its porous structure. Notably, high-silica fly ash, with a SiO_2 content exceeding 50%, possesses considerable potential as a cost-effective natural silicon source for the synthesis of mesoporous silicon-based materials. Deshannavar B. U.[18] et al. utilized high-silica fly ash as an adsorbent for the removal of Reactive Blue 25 dye from aqueous solutions, achieving a removal capacity of 8.17 mg g^{-1}. However, the adsorption capacity of raw high-silica fly ash remains limited and generally requires activation via physical or chemical modification. Hussain Z.[19] modified fly ash with NaOH and HCl, obtaining maximum removal efficiencies of 96.03% for Direct Red 4BS and 93.82% for Direct Lake Blue 5B under optimal conditions. Although acid and alkali modifications can improve surface properties, they often demand stringent reaction conditions and may reduce the activity of silicon and aluminum. Chen et al.[20] synthesized NaP1 zeolite by hydrothermal method to degrade methylene blue. While high-temperature modification effectively reduces waste volume, it is energy-intensive and may cause secondary pollution. Although the research on fly ash as an adsorbent has been reported, how to design efficient modification strategies for specific pollutants and systematically compare the advantages and disadvantages of different modification paths is still a weak link in current research. The methods of alkali activation, zeolite synthesis and surfactant modification of fly ash have been widely explored. Yunxin Xie et al.[21] fly ash were used to synthesize zeolite molecular sieve. The results showed that the zeolite molecular sieve extracted from fly ash showed good activity in adsorbing and removing ammonia nitrogen in wastewater. Additionally, Subhajit Dash et al.[22] prepared sulfonic acid-functionalized fly ash via condensation with 3-mercaptopropyltrimethoxysilane and subsequent oxidation with H_2O_2, achieving removal efficiencies of 99.20% for malachite green and 98.70% for rhodamine 6G. These findings highlight the potential of fly ash as a base material for the development of novel, eco-friendly, and efficient adsorbents. However, most of these studies focused on the optimization of a single modification route.

Mesoporous silicon-based materials have been widely employed as adsorbents and catalyst supports in the field of environmental remediation due to their ordered pore structures and tunable surface properties. Fashandi et al.[23] prepared mesoporous silicon-based materials using organosilicate salts

as the silicon source. However, the synthesis of conventional mesoporous materials typically relies on expensive silicon sources, resulting in high production costs. Consequently, research efforts have primarily focused on identifying more economical silicon sources and developing simpler synthesis processes. Renata Jarosz et al.[24] produced novel zeolite composites using fly ash and lignite, demonstrating the potential for industrial solid wastes to substitute for toxic organosilicon compounds. Naruemon Setthaya et al.[25] used a variety of metakaolin and fly ash mixed by impregnation method to obtain TiO-containing mesoporous silica-based materials containing titanium dioxide for the removal of methylene blue. Therefore, to develop green synthesis methods for mesoporous silicon-based materials, high-silica fly ash is being considered as a silicon source, with ultrasonic-assisted and alkali fusion–hydrothermal methods used for preparation. In addition to mesoporous silicon-based materials, surface-modified materials utilizing alkyl modifiers have also been extensively studied. Deng Hui et al.[26] Synthesized a novel modified zeolite by co-supporting cetyltrimethylammonium and titanium dioxide onto fly ash-derived zeolites, achieving removal rates of X-3B dye in aqueous solution consistently above 96%. Notably, materials modified with sodium dodecyl sulfate as the surface modifier have demonstrated effective removal of environmental pollutants. Hence, fly ash, as an abundant and inexpensive solid waste, especially high-silica fly ash (SiO_2 content > 50%), holds great promise as a silicon source for the preparation of mesoporous silicon-based and surface-modified materials, significantly enhancing its adsorption properties and enabling high-value utilization.

Based on this, this study developed an ultrasonic-assisted alkali fusion–hydrothermal synthesis method for the preparation of mesoporous silica-alumina materials (MSAM) using high-silica fly ash with SiO_2 content greater than 50% as the silicon source. Ultrasonic treatment not only enhances the mixing efficiency of the precursor, but also optimizes the nucleation process as a key step, thereby successfully constructing a mesoporous structure with a high specific surface area (48.92 m^2 g^{-1}) under relatively mild hydrothermal conditions (100 °C, 8 h). This combination strategy of ultrasound-assisted and mild hydrothermal conditions effectively reduces energy consumption while ensuring structural order, which is an improvement of the traditional high-temperature and high-pressure hydrothermal method. At the same time, we developed a sodium dodecyl sulfate (SDS) surface modified fly ash (SDS/FA) process in parallel. In this study, an integrated modification strategy (ultrasonic-assisted alkali fusion–hydrothermal method) and a key application verification link (dynamic column experiment) were organically combined to systematically answer the practical scientific question of 'how to select the most suitable fly ash high-value path for specific dyes'.

2 Materials and methods

2.1. Experimental materials

The fly ash used in the experiments was Class F fly ash obtained from a power plant in Fuxin City (42.01°N, 121.65°E). The ash

was sieved to a particle size of 90 to 120 mesh, the fly ash after pretreatment was washed three times with deionized water,[27] and then dried in a forced air drying oven (DHG-9030, Shanghai Yiheng Scientific Instrument Co. Ltd, China) at 378.15 K for subsequent use. The major chemical components of the coal gangue were determined by X-ray fluorescence spectroscopy (XRF), and the results are shown in Table 1.

The following reagents were used in the experiments: NaOH, HNO$_3$, sodium dodecyl sulfate (SDS), ethanol, methylene blue, and methyl violet. All reagents were of analytical grade and sourced from China National Pharmaceutical Group Corporation (Shanghai, China). Deionized water was used throughout the entire experimental process.

2.1.1. Simulated MB and MV wastewater. The concentrations of the simulated pollutants were prepared based on the actual wastewater quality from a textile dyeing park. The initial dye concentration is set to 100 mg L^{-1}, which is within the typical range (50–200 mg L^{-1}) of the simulated actual textile wastewater secondary effluent.[28] It is also suitable for accurate spectral determination and easy to compare with a large number of published adsorption studies. The stock solutions were then diluted with deionized water to obtain solutions of various concentrations, as required for the experiments. The pH of the solutions was adjusted using 0.1 mol per L HNO$_3$ and 0.1 mol per L NaOH.

2.2. Experimental methods

2.2.1. Preparation of MSAM and SDS/FA

2.2.1.1 MSAM. A precise amount of 5 g of dried fly ash was weighed and placed in a crucible. NaOH was then added in a 1.2 : 1 ratio, and the mixture was thoroughly blended with the fly ash. After vigorous stirring, the mixture was transferred to a muffle furnace and heated at a rate of 10 °C per minute to 550 °C, where it was maintained for 60 min to complete the alkali fusion process. Upon completion of the reaction, the molten substance was removed and allowed to cool to ambient temperature. It was then ground to a particle size range of 0.25–0.38 mm and mixed with distilled water before being stirred for 2 h. The mixture was subjected to ultrasonic treatment for a specified duration using a bath-type ultrasonic cleaner operating at 40 kHz and 240 W power. Afterward, it was aged at room temperature for 20 h. The resulting white gel was transferred to a 100 mL stainless steel hydrothermal reactor and subjected to hydrothermal treatment at 100 °C for a specific period. Following the reaction, the product was cooled to room temperature, filtered, and washed with deionized water until the pH reached 8. Finally, it was dried to constant weight in an electric hot air drying oven at 80 °C, yielding the fly ash-based mesoporous silicon–aluminum material. The material was then ground, sieved, and stored properly for subsequent experimental use.

2.2.1.2 SDS/FA. A precisely weighed amount of 10 g of fly ash with a particle size of 0.25–0.38 mm was placed in a beaker, and 200 mL of distilled water was added to achieve uniform dispersion. The beaker was then placed in a water bath at 60 °C for heating. During this process, 3 g of sodium dodecyl sulfate was added to the solution and treated with ultrasonic cleaning at 40 kHz for 15 min. After the ultrasonic treatment, the mixture was subjected to oscillation for 8 h to promote the reaction, followed by standing to allow phase separation. The upper clear liquid was then decanted. The mixture was repeatedly washed with distilled water until the wash liquid approached neutrality. The modified fly ash was then placed in a forced-air drying oven at 95 °C for drying. Once dried, the modified fly ash was ground, sieved, and properly stored for subsequent experimental use.

2.2.2. Single factor test. The level range of the single factor test was determined based on the pre-experimental results and the existing literature.[29] The setting of alkali–cement ratio (0.4 : 1–2.0 : 1) covers the critical range from incomplete dissolution of silicon–aluminum components to excessive alkali that may lead to structural collapse. The setting of ultrasonic time (5–25 min) was designed to explore the effect of optimizing gel mixing and nucleation through cavitation effect. After more than 25 min, too long ultrasound may cause damage to the formed structure. Therefore to determine the optimal conditions for the preparation of MSAM and SDS/FA using modified high-silica fly ash, the preparation conditions for both materials were compared. The preparation of MSAM was investigated using a single-factor method, considering four factors: the mass ratio of NaOH to fly ash (0.4 : 1, 0.8 : 1, 1.2 : 1, 1.6 : 1, 2.0 : 1), ultrasonic treatment time (5, 10, 15, 20, 25 min), hydrothermal treatment time (4, 6, 8, 10, 12 h), and hydrothermal temperature (60, 80, 100, 120, 140 °C). The fly ash-based adsorbent material was then added to MB and MV wastewater at a solid-to-liquid ratio of 1 : 200 (g mL^{-1}) and agitated at 300 rpm, with regular sampling. The removal efficiencies of MB and MV were used as indicators to evaluate and identify the optimal preparation conditions for the fly ash-based adsorbent.

The preparation of SDS/FA was investigated using a single-factor method to examine the effects of four factors: the particle size of fly ash (0.5–0.7, 0.38–0.5, 0.25–0.38, 0.18–0.25, 0.15–0.18 mm), SDS dosage (1, 2, 3, 4, 5 g), ultrasonic treatment time (10, 15, 20, 25, 30 min), and oscillation time (4, 6, 8, 10, 12 h) on the removal of MB and MV from wastewater by SDS/FA. The SDS/FA was added to MB and MV wastewater at a solid-to-liquid ratio of 1 : 200 (g mL^{-1}), and the mixture was agitated at 300 rpm, with samples being taken at regular intervals. The removal efficiencies of MB and MV were used as the evaluation criteria to determine the optimal preparation conditions for the modified fly ash.

2.2.3. Response surface experiment. Based on the single-factor experiments, a response surface optimization design

Table 1 Main compositions of fly ash

Component	SiO$_2$	TiO$_2$	Al$_2$O$_3$	Fe$_2$O$_3$	MnO	MgO	CaO	Na$_2$O	K$_2$O	P$_2$O$_5$
Content (%)	67.10	0.12	19.74	3.35	0.34	2.87	4.00	1.08	1.30	0.10

Table 2 Level of impact factors and coding

Factor	Coding	Level −1	0	1
Alkali ash ratio	X_1	0.8	1.2	1.6
Ultrasonic time (min)	X_2	15	20	25
Hydrothermal time (h)	X_3	6	8	10
Hydrothermal reaction temperature (°C)	X_4	80	100	120

was performed using three levels for four factors: the alkali-to-ash ratio, ultrasonic time, hydrothermal time, and hydrothermal temperature. The levels of the experimental factors and their design are presented in Table 2.

Based on the single-factor experiments, a response surface optimization design was conducted using three levels for four factors: fly ash particle size, SDS dosage, ultrasonic time, and oscillation time. The levels of the experimental factors and their design are presented in Table 3.

2.2.4. Adsorption test. In this study, methylene blue (MB) and methyl violet (MV) solutions were used to simulate industrial dye wastewater, and the adsorption performance of fly ash-based adsorbents was evaluated. Firstly, MSAM and SDS/FA were added to MB and MV wastewater at a solid–liquid ratio of 1 : 200 (g mL^{-1}), oscillated at a speed of 300 rpm, and sampled regularly. The residual concentrations of MB and MV were measured using a 721 UV-Vis spectrophotometer at wavelengths of 666 nm and 617 nm, respectively. The removal efficiency (R, %) was calculated using the following formula:

$$\eta = \frac{C_0 - C_t}{C_0} \times 100\%$$ (1)

where: η is the removal rate, %; C_0 and C_t represent the initial and residual concentrations of the target ions, respectively, mg L^{-1}.

2.2.5. Leaching toxicity test method. By the "Toxic Leaching Method for Solid Waste – Sulfuric Nitric Acid Method" (HJ/T300-2007), sulfuric acid and nitric acid with a mass ratio of 2 : 1 were added to deionized water to make the solution pH 3.1–3.3, phosphate buffer solution to make the solution pH 7.0–7.2, and carbonate buffer solution to make the solution pH 9.0–9.2. The dried fly ash, MSAM, and SDS/FA were then added to the extraction solution at a solid-to-liquid ratio of 1 : 10 (g mL^{-1}) and stirred for 18 h at room temperature. The concentrations of the major heavy metal ions were determined using a flame atomic absorption spectrometer. Three parallel samples were

prepared for each group, and the average value was used as the result.

2.2.6. Regeneration test of MSAM and SDS/FA. The reusability of MSAM and SDS/FA was evaluated through three cycles of adsorption–desorption experiments. In each cycle, 200 mL of simulated MB and MV wastewater was mixed with 2 g L^{-1} of the MSAM and SDS/FA adsorbents, and the mixture was stirred at 300 rpm for 180 minutes at room temperature to complete the adsorption process. Afterward, desorption was performed using a 0.5 mol per L EDTA solution, with stirring for 3 h. Upon completion of desorption, the adsorbents were separated by centrifugation, washed, and dried to be reused in the adsorption experiments for MB and MV under the same conditions. Three parallel samples were prepared for each group, and the average value was used as the result.

2.2.7. Material characterization methods. The surface morphology of the materials was analyzed using scanning electron microscopy coupled with energy-dispersive spectroscopy (SEM-EDS, SIGMA 500, Carl Zeiss AG, Germany). Measurements were conducted at 10 μA current, 15 kV accelerating voltage, under argon protection, with magnification ranging from 5000× to 10 000×. X-ray diffraction (XRD, D8 ADVANCE, Bruker Corporation, Germany) was employed for mineralogical composition analysis and crystal structure determination. The measurements used a Cu-Kα radiation source (40 kV, 30 mA) with a scanning range of $2\theta = 10–90°$, step size of 0.02°, and scanning speed of 0.5 s per step. Fourier-transform infrared spectroscopy (FTIR, VERTEX 70, Bruker Corporation, Germany) was utilized to identify surface functional groups. Samples were dried, ground to <0.074 mm, mixed with KBr at a 1 : 100 ratio, and pressed into pellets. Spectra were recorded in the 400–4000 cm^{-1} wavenumber range. The specific surface area and pore size distribution were determined via the Brunauer–Emmett–Teller (BET) method using a Micromeritics ASAP 2460 analyzer (Micromeritics Instrument Ltd, USA). Samples were degassed at 200 °C for 6 h under vacuum before N$_2$ adsorption measurements.

2.2.8. Dynamic test methodology. A detailed comparison and analysis were conducted on the application of two fly ash-based modified materials, MSAM and SDS/FA, in treating MB and MV simulated dye wastewater. The results demonstrated that SDS/FA exhibited higher removal efficiency and better pH stability. Additionally, the preparation process of SDS/FA was relatively simple, more cost-effective, and easier to scale up for production. Therefore, to further validate the performance of SDS/FA in practical applications, as well as to investigate its stability and durability under dynamic conditions, dynamic column experiments will be conducted in this chapter. These experiments aim to simulate the conditions of real wastewater treatment processes and evaluate the removal efficiency of SDS/FA for MB and MV in a continuous flow system. The study in this chapter will primarily focus on the design of the experimental setup, the experimental methodology, and the analysis of the dynamic test results, including the dynamic changes in the removal efficiency of SDS/FA for the dyes and their pH adjustment capabilities. Through these comprehensive studies, a more accurate prediction of the material's performance in

Table 3 Level of impact factors and coding

Factor	Coding	Level −1	0	1
Fly ash particle size (mm)	X_1	0.16	0.24	0.32
SDS dosage (g)	X_2	2	3	4
Ultrasonic time (min)	X_3	15	20	25
Shaking time (h)	X_4	6	8	10

real-world applications will be made, providing a scientific basis for its potential use in industrial wastewater treatment.

Based on the results of single-factor experiments and response surface optimization, SDS/FA was prepared. Simulated wastewater containing MB and MV at concentrations of 100 mg L^{-1} and pH 8 was prepared according to the static test results. Simulated wastewater was continuously fed into the dynamic column by the experimental design. The dynamic column operated at room temperature for 28 days, with pH, MB, and MV concentrations measured every 12 h.

To simulate real-world application scenarios, a dynamic column test system for the removal of MB and MV from wastewater using SDS/FA was constructed, as shown in Fig. 1. The system consisted of six acrylic tubes with an inner diameter of 50 mm and a height of 500 mm. Columns 1 and 3 were filled with fly ash particles of particle size 0.25–0.38 mm, while columns 2 and 4 were filled with the prepared SDS/FA, with a packing height of 250 mm for all columns. A peristaltic pump was used to introduce 100 mg per L simulated MB and MV wastewater into the dynamic columns through the lower inlet. The hydraulic retention time was controlled at 150 min. This allowed sufficient contact between the MB and MV in the solution and the materials, enabling the dynamic adsorption experiments. The concentrations of MB and MV in the effluent were collected and analyzed, and pH changes were recorded. Glass beads, which had been acid-washed, alkali-washed, and rinsed with deionized water, were used as the buffering medium at both the top and bottom of the columns, with nylon filtration membranes placed in between. After assembly, deionized water was pumped into the system to eliminate air and ensure stable saturation within the columns, avoiding preferential flow. Water samples were taken every 12 h to measure pH and the concentrations of MB and MV. Each group of experiments was repeated three times, with the average value used to calculate the removal efficiency (η). The experimental setup is shown in Fig. 1.

3 Results and discussion

3.1. Single-factor test analysis

3.1.1. Comprehensive optimization and synergistic effect of MSAM preparation conditions. During the preparation of MSAM, four key factors—alkali-to-ash ratio, ultrasonic time, hydrothermal time, and hydrothermal temperature are interrelated and collectively determine the formation of the

mesoporous structure and the dye adsorption performance of the material. As shown in Fig. 2(a) and (b), the removal efficiency of MB and MV increases initially and then decreases as the alkali-to-ash ratio increases. When the alkali-to-ash ratio is 1.2 : 1, the removal efficiencies for MB and MV reach 94.70% and 80.05%, respectively. This is because the alkali-to-ash ratio directly affects the dissolution–polymerization equilibrium of silicon and aluminum elements by regulating the system's pH, with an appropriate alkalinity promoting the complete dissolution of the silico-aluminate precursor while preventing excess Na$^+$ from occupying active sites, thus providing an ideal reactant ratio for the subsequent hydrothermal process.[30,31] As shown in Fig. 2(c) and (d), the removal efficiencies of MB and MV show an initial increase followed by a decrease as ultrasonic time increases. The highest removal efficiencies of 94.70% and 80.05% for MB and MV are reached after 15 min of ultrasound. This is because ultrasound treatment, through cavitation effects, achieves dual functions: on one hand, it accelerates the uniform mixing of silicon and aluminum components, making the gel's silicon–aluminum ratio closer to the raw material ratio; on the other hand, the microbubbles generated serve as nucleation sites, shortening the crystallization induction period.[32] As shown in Fig. 2(e) and (f), the removal efficiencies of MB and MV also show an initial increase followed by a decrease as hydrothermal time is extended. When the hydrothermal time is 8 hours, the removal efficiencies for MB and MV reach 94.70% and 80.05%, respectively. This is due to the two-stage process of crystal formation in MSAM: the nucleation induction stage and the crystal growth stage. In the nucleation induction stage, nuclei begin to form and grow, and once the nuclei exceed a critical size, the crystal growth stage begins, during which the crystals rapidly expand, and the conversion efficiency of the raw materials increases.[33] As seen in Fig. 2(g) and (h), as hydrothermal temperature increases, the removal efficiencies of MB and MV initially increase and then decrease. The highest removal efficiencies of 94.70% and 80.05% for MB and MV are achieved at a hydrothermal temperature of 100 °C. This is because higher hydrothermal temperatures result in a more concentrated pore size distribution, significantly increasing the specific surface area and pore volume of MSAM. However, excessively high temperatures can affect the re-hydrolysis, crosslinking, and uniform distribution of silicon components, destabilizing the mesoporous structure and leading to uneven pore distribution or pore collapse.[34] At an alkali-to-ash ratio of 1.2 : 1, ultrasonic time of 15 min, hydrothermal time of 8 h, and
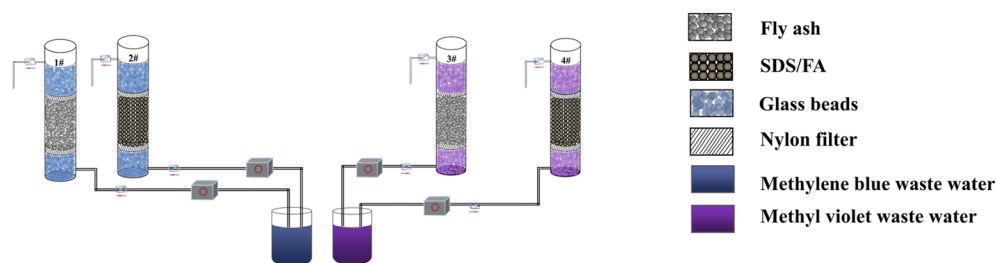

Fig. 1 SDS/FA dynamic test device system.

Fly ash
SDS/FA
Glass beads
Nylon filter
Methylene blue waste water
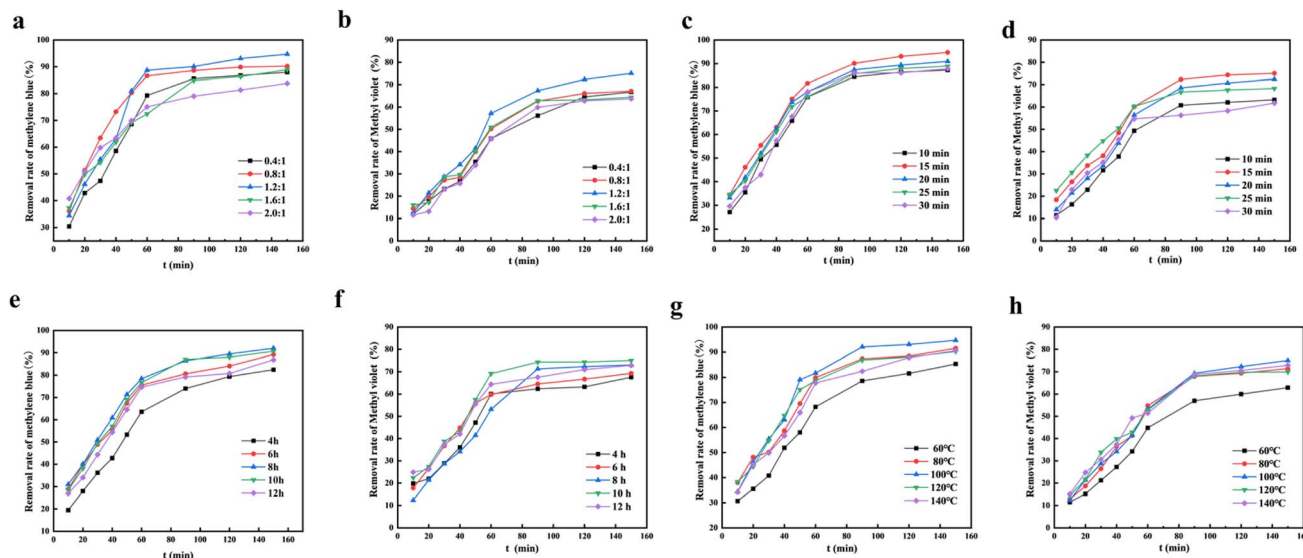Methyl violet waste water

Fig. 2 Single factor diagram of MSAM. (a) and (b) Alkali–cement ratio (ultrasonic time: 15 min, hydrothermal time: 8 h, hydrothermal temperature: 100 °C, stirring speed: 300 rpm). (c) and (d) Ultrasonic time (alkali–cement ratio: 1.2 : 1, hydrothermal time: 8 h, hydrothermal temperature: 100 °C, stirring speed: 300 rpm). (e) and (f) Hydrothermal time (alkali–cement ratio: 1.2 : 1, ultrasonic time: 15 min, hydrothermal temperature: 100 °C, stirring speed: 300 rpm). (g) and (h) Hydrothermal temperature (alkali–cement ratio: 1.2 : 1, ultrasonic time: 15 min, hydrothermal time: 8 h, stirring speed: 300 rpm).

hydrothermal temperature of 100 °C, the removal efficiencies of MB and MV reach 94.70% and 80.05%, respectively. This performance improvement can be attributed to the synergistic optimization of the silicon–aluminum ratio by the alkali-to-ash ratio and ultrasound, which provides abundant surface hydroxyl sites, and the mesoporous structure controlled by the hydrothermal temperature–time coupling, which enhances the diffusion and capture efficiency of the dyes. The 100 °C thermodynamic conditions ensure the directional assembly of silico-aluminates, forming a mesoporous structure with a concentrated pore size distribution. The 8 h duration ensures sufficient crystal growth while avoiding phase changes or pore collapse that may occur with excessively long durations.

3.1.2. Comprehensive optimization and synergistic effect of SDS/FA preparation conditions. During the preparation of the SDS/FA composite adsorbent, four key parameters—fly ash particle size, SDS dosage, ultrasonic time, and oscillation time—work synergistically to regulate the material's surface characteristics and dye adsorption performance. As shown in Fig. 3(a) and (b), with decreasing fly ash particle size, the removal efficiency of SDS/FA for MB and MV increases initially and then decreases. When the fly ash particle size is in the range of 0.25–0.38 mm, the removal efficiencies for MB and MV can reach 85.23% and 91.17%, respectively. This is because smaller particle sizes result in larger specific surface areas, which enhance the adsorption capacity for MB and MV.[35,36] As the specific surface area of fly ash increases, the number of available adsorption sites also increases, allowing for a greater load of SDS molecules. As shown in Fig. 3(c) and (d), with an increase in SDS dosage, the removal efficiencies of SDS/FA for MB and MV also increase. At an SDS dosage of 3 g, the removal efficiencies for MB and MV reach 85.67% and 95.38%, respectively.

This is because the anionic groups attached to the fly ash surface increase with higher SDS concentrations, which enhances the adsorption efficiency through network trapping.[37,38] As shown in Fig. 3(e) and (f), ultrasonic treatment for 5–15 min increases the removal efficiency of SDS/FA, but when the time extends to 15–30 min, the removal efficiency decreases. The highest removal efficiencies of 85.7% for MB and 92.52% for MV are achieved after 15 min of ultrasonic treatment. This is because ultrasound facilitates the binding and exchange of SDS molecules with fly ash, resulting in a more uniform distribution of SDS on the fly ash surface, which increases the removal efficiency of MB and MV. However, excessively long ultrasonic times lead to desorption of the surfactant, causing a decrease in removal efficiency.[39] As shown in Fig. 3(g) and (h), the removal efficiencies of MB and MV increase with longer oscillation time. When the modification time is 8 h, the highest removal efficiencies of 85.76% and 91.45% for MB and MV are achieved. This is because the adsorption of SDS on the fly ash surface requires a certain amount of time to reach equilibrium. As the oscillation time increases, the removal efficiency for MB and MV first increases and then decreases. This is because, after the SDS reaches saturation on the fly ash surface, a brief desorption occurs, and excessive oscillation time can lead to partial SDS desorption, resulting in decreased removal efficiency.[40,41] At a fly ash particle size of 0.25–0.38 mm, SDS dosage of 3 g, ultrasonic time of 15 minutes, and modification time of 8 hours, SDS/FA achieves removal efficiencies of 85.67% and 95.38% for MB and MV, respectively. The performance enhancement can be attributed to the synergistic mechanism of "carrier construction—surface modification—kinetic optimization" driven by these four factors. The selection of particle size determines the physical characteristics of the carrier, SDS dosage controls the
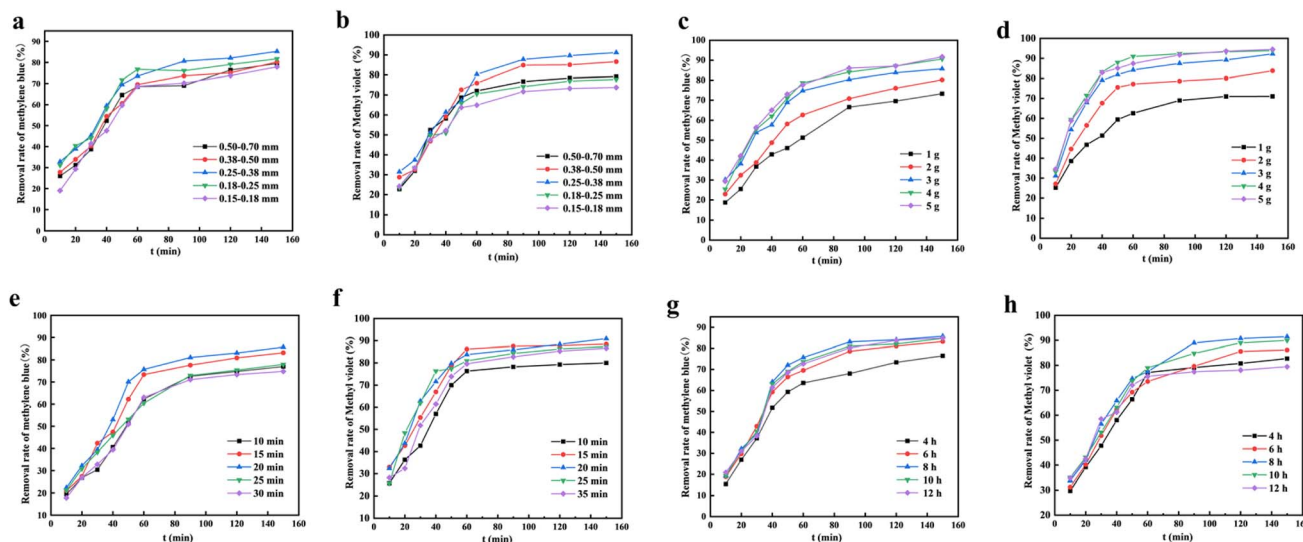
Fig. 3 Single factor diagram of SDS/FA. (a) and (b) Fly ash fraction (SDS dosage: 3 g, ultrasonic time: 20 min, oscillation time: 8 h, stirring speed: 300 rpm). (c) and (d) SDS dosage (fly ash fraction: 0.25–0.38 mm, ultrasonic time: 20 min, oscillation time: 8 h, stirring speed: 300 rpm). (e) and (f) Ultrasonic time (fly ash fraction: 0.25–0.38 mm, SDS dosage: 3 g, oscillation time: 8 h, stirring speed: 300 rpm). (g) and (h) Oscillation time (fly ash fraction: 0.25–0.38 mm, SDS dosage: 3 g, ultrasonic time: 20 min, stirring speed: 300 rpm).

extent of chemical modification, and the synergy between ultrasound and oscillation optimizes the kinetics of the modification process.[42]

3.2. Response surface test analysis

3.2.1. The removal rate of MB and MV under different preparation conditions of MSAM and SDS/FA was analyzed. A total of 29 interaction experiments were designed using Design-Expert 13.0 software, with the removal efficiencies of MB and MV at 150 min, when equilibrium was reached, being taken as the response values. The experimental design and results are presented in Tables 4–9.

3.2.1.1 MB removal rate analysis. For MSAM materials, it was found that there was a significant synergistic effect between alkali–cement ratio, ultrasonic time, hydrothermal time and hydrothermal temperature. It can be seen from Fig. 4(a) that the interaction between alkali–cement ratio and ultrasonic time was not significant ($P = 0.1924 > 0.05$), and the alkali–cement ratio was dominant. It can be seen from Fig. 4(b) that the interaction between alkali–cement ratio and hydrothermal time was significant ($P = 0.0005 < 0.05$). The MB removal rate increased first and then decreased with the increase of the two factors. It can be seen from Fig. 4(c) that the interaction between alkali–cement ratio and hydrothermal temperature is extremely significant ($P < 0.0001$), and the order of significance is: alkali–ash ratio > hydrothermal temperature. The MB removal rate increased first and then decreased with the increase of the two factors. It can be seen from Fig. 4(d) that the interaction between ultrasonic time and hydrothermal time was significant ($P = 0.0239$). The order of significance is hydrothermal time > ultrasonic time, and the MB removal rate increases first and then decreases with the increase of the two factors. It can be seen from Fig. 4(e) that the interaction between ultrasonic time

Table 4 Experimental design factors and results[a]

Numbering	A	B	C	D	MB removal rate (%)	MV removal rate (%)
1	1.2	10	6	100	87.60	60.48
2	1.2	15	6	120	87.75	61.63
3	1.2	15	8	100	93.15	75.14
4	1.2	15	8	100	93.15	75.14
5	1.6	10	8	100	91.90	63.70
6	1.6	15	8	80	90.05	64.85
7	1.6	15	10	100	92.20	66.00
8	1.2	20	8	120	87.55	60.36
9	1.2	10	10	100	86.50	59.32
10	1.6	20	8	100	91.35	68.08
11	1.2	15	8	100	93.15	75.14
12	1.2	15	8	100	93.15	75.14
13	0.8	15	10	100	84.75	57.60
14	1.2	15	6	80	85.90	58.75
15	1.2	15	10	120	86.05	59.91
16	0.8	20	8	100	88.25	62.03
17	1.2	20	8	80	87.40	60.47
18	1.2	10	8	120	86.55	59.58
19	1.2	20	10	100	88.70	62.69
20	1.2	10	8	80	85.75	60.80
21	1.2	20	6	100	87.90	61.91
22	1.6	15	8	120	90.95	66.08
23	0.8	15	8	80	85.10	58.12
24	1.2	15	10	80	86.25	59.27
25	0.8	10	8	100	85.50	56.59
26	0.8	15	8	120	85.65	58.64
27	0.8	15	6	100	88.80	63.81
28	1.6	15	6	100	90.15	75.14
29	1.2	15	8	100	93.15	75.14

[a] *A* is the ratio of alkali to ash; *B* is the ultrasonic time, min; *C* is the hydrothermal time, h; *D* is the hydrothermal temperature, °C.

Table 5 ANOVA table for the second-order model of MB removal rate[a]

Source of variance	Quadratic sum	Degree of freedom	Mean square value	F ratio	P ratio	Significance
Model	229.73	14	16.41	304.45	<0.0001	Significant
A-Alkali ash ratio	67.93	1	67.93	1260.24	<0.0001	***
B-Ultrasonic time	4.50	1	4.50	83.52	<0.0001	***
C-Hydrothermal time	1.11	1	1.11	20.60	0.0005	**
D-Hydrothermal reaction temperature	1.37	1	1.37	25.36	0.0002	**
AB	2.72	1	2.72	50.51	<0.0001	***
AC	9.30	1	9.30	172.59	<0.0001	***
AD	0.0306	1	0.0306	0.5682	0.4635	⊙
BC	0.9025	1	0.9025	16.74	0.0011	**
BD	0.1056	1	0.1056	1.96	0.1833	⊙
CD	1.05	1	1.05	19.49	0.0006	**
A^2	11.82	1	11.82	219.33	<0.0001	***
B^2	42.59	1	42.59	790.24	<0.0001	***
C^2	53.15	1	53.15	986.10	<0.0001	***
D^2	94.28	1	94.28	1749.24	<0.0001	***
Residual error	0.7546	14	0.0539			
Lack of fit	0.7546	10	0.0755			
Pure error	0.0000	4	0.0000			
Total dispersion	230.49	28				

[a] ***, $P < 0.001$, extremely significant; **, $P < 0.01$, highly significant; *, $P < 0.05$, significant; ⊙, non-significant.

and hydrothermal temperature was extremely significant ($P = 0.0001 < 0.05$). The MB removal rate increased first and then decreased with the increase of the two factors. It can be seen from Fig. 4(f) that the interaction between hydrothermal time and hydrothermal temperature was significant ($P = 0.0013$). The MB removal rate increased first and then decreased with the increase of the two factors. Experiments show that the alkali–cement ratio is the key dominant factor. The optimum value is 1.2 : 1, at this time, the silicon–aluminum precursor is fully dissolved, which is conducive to the formation of mesoporous structure; excessive alkali (Na) will occupy the polymerization

site, resulting in a decrease in performance. The specific surface area of MSAM prepared under the optimal conditions (alkali–cement ratio 1.2 : 1, ultrasonic 20 min, hydrothermal 8 h, 100 °C) reached 48.92 m^2 g^{-1}, and the XRD pattern showed good structural order. This indicates that the crystallinity and porosity of the mesoporous structure have reached a better balance. The results showed that the removal rate of MB was up to 93.87% and the adsorption capacity was 18.774 mg g^{-1} under the optimal conditions.

For SDS/FA materials, fly ash particle size (0.25–0.38 mm), SDS dosage (3 g), ultrasonic time (15 min) and oscillation time

Table 6 ANOVA table for the second-order model of MV removal rate

Source of variance	Quadratic sum	degree of freedom	Mean square value	F ratio	P ratio	Significance
Model	895.79	14	63.98	478.20	<0.0001	Significant
A-Alkali ash ratio	102.43	1	102.43	765.56	<0.0001	***
B-Ultrasonic time	12.14	1	12.14	90.73	<0.0001	***
C-Hydrothermal time	1.29	1	1.29	9.62	0.0078	**
D-Hydrothermal reaction temperature	11.88	1	11.88	88.79	<0.0001	***
AB	2.34	1	2.34	17.50	0.0009	**
AC	6.43	1	6.43	48.03	<0.0001	***
AD	0.4160	1	0.4160	3.11	0.0997	⊙
BC	2.16	1	2.16	16.15	0.0013	**
BD	5.98	1	5.98	44.68	<0.0001	***
CD	1.25	1	1.25	9.37	0.0084	**
A^2	158.32	1	158.32	1183.23	<0.0001	***
B^2	188.74	1	188.74	1410.56	<0.0001	***
C^2	423.65	1	423.65	3166.25	<0.0001	***
D^2	361.27	1	361.27	2699.98	<0.0001	***
Residual error	1.87	14	0.1338			
Lack of fit	1.87	10	0.1873			
Pure error	0.0000	4	0.0000			
Total dispersion	897.66	28				

RSC Advances | Paper

Open Access Article. Published on 06 October 2025. Downloaded on 2/12/2026 5:26:33 AM. This article is licensed under a Creative Commons Attribution-NonCommercial 3.0 Unported Licence.

Table 7 Experimental design factors and results

Numbering	A	B	C	D	MB removal rate (%)	MV removal rate (%)
1	0.32	4	20	4	82.16	92.48
2	0.32	4	10	8	82.45	92.17
3	0.24	3	15	6	85.33	94.16
4	0.24	3	15	6	85.21	94.15
5	0.16	2	10	4	82.47	77.84
6	0.24	3	15	10	77.26	74.73
7	0.32	2	10	8	72.28	81.5
8	0.16	2	20	8	67.76	78.39
9	0.24	3	15	6	85.15	94.16
10	0.40	3	15	6	77.37	88.05
11	0.16	4	10	4	65.83	73.92
12	0.08	3	15	6	68.42	75.31
13	0.24	5	15	6	72.78	91.61
14	0.32	4	10	4	81.70	89.28
15	0.32	2	10	4	79.22	84.85
16	0.32	4	20	8	82.79	86.37
17	0.24	3	15	6	85.24	94.16
18	0.32	2	20	4	67.22	85.61
19	0.16	4	10	8	66.75	78.52
20	0.24	3	15	6	85.24	94.16
21	0.24	3	15	6	82.28	90.83
22	0.24	3	15	2	82.88	80.05
23	0.24	1	15	6	66.31	80.40
24	0.16	4	20	8	67.46	80.96
25	0.16	2	20	4	72.38	88.49
26	0.32	2	20	8	60.29	72.61
27	0.16	2	10	8	78.32	78.92
28	0.24	3	25	6	64.79	88.14
29	0.16	4	20	4	67.20	87.35
30	0.24	3	5	6	78.25	87.24

(8 h) showed a significant synergistic effect. From Fig. 4(g), it can be seen that the interaction between fly ash particle size and SDS dosage is extremely significant ($P < 0.05$). It can be seen

from Fig. 4(i) that the interaction between fly ash particle size and oscillation time is not significant ($P = 0.2360 > 0.05$). It can be seen from Fig. 4(j) that the interaction between SDS dosage and ultrasonic time was extremely significant ($P < 0.0001$). The removal rate of MB increased with the increase of SDS dosage, and increased first and then decreased with the extension of ultrasonic time. It can be seen from Fig. 4(k) that the interaction between SDS dosage and oscillation time was extremely significant ($P < 0.0001$). The effect of SDS dosage and oscillation time on MB removal rate was the same. It can be seen from Fig. 4(l) that the interaction between ultrasonic time and oscillation time was not significant ($P = 0.7590 > 0.05$). With the extension of oscillation time and ultrasonic time, the removal rate of MB increased first and then decreased. When the oscillation time exceeds a certain critical point, the removal rate begins to decrease, which is due to the fact that the physical structure of the adsorbent changes due to too long oscillation, or the adsorption site tends to be saturated. Experiments show that SDS dosage is the key dominant factor affecting the modification effect. The optimal value is 3 g, and SDS molecules can form a complete monolayer coverage on the surface of fly ash, effectively introducing hydrophobic functional groups. Insufficient dosage will lead to incomplete modification, while excessive SDS may form micelles, which will reduce the effective adsorption sites. The specific surface area of SDS/FA prepared under the optimal conditions (SDS dosage 3 g, ultrasonic 15 min, oscillation 8 h) was significantly increased to 93.59 m² g⁻¹. However, the samples prepared by deviating from this condition showed SDS agglomeration or uneven coverage, and the specific surface area growth was limited. This indicates that the optimization of surfactant coverage and interface properties has reached the best balance. The results showed that the removal rate of MB was up to 83.46% and the adsorption capacity was 16.692 mg g⁻¹ under the optimal conditions.

Table 8 ANOVA table for the second-order model of MB removal rate

Source of variance	Quadratic sum	Degree of freedom	Mean square value	F ratio	P ratio	Significance
Model	1766.38	14	126.17	128.12	<0.0001	Significant
A-Fly ash particle size	139.39	1	139.39	141.55	<0.0001	***
B-SDS dosage	35.87	1	35.87	36.42	<0.0001	***
C-Ultrasonic time	196.54	1	196.54	199.58	<0.0001	**
D-Shaking time	40.87	1	40.87	41.51	<0.0001	**
AB	438.69	1	438.69	445.49	<0.0001	***
AC	1.33	1	1.33	1.35	0.2626	⊙
AD	1.50	1	1.50	1.52	0.2360	⊙
BC	141.13	1	141.13	143.32	<0.0001	***
BD	39.69	1	39.69	40.30	<0.0001	***
CD	0.0961	1	0.0961	0.0976	0.7590	⊙
A^2	240.32	1	240.32	244.04	<0.0001	***
B^2	395.55	1	395.55	401.67	<0.0001	***
C^2	299.38	1	299.38	304.01	<0.0001	***
D^2	37.31	1	37.31	37.88	<0.0001	***
Residual error	14.77	15	0.9847			
Lack of fit	7.48	10	0.7483	0.5133	0.8272	⊙
Pure error	7.29	5	1.46			
Total dispersion	1781.15	29				

© 2025 The Author(s). Published by the Royal Society of Chemistry

Table 9 ANOVA table for second order model of MV removal rate

Source of variance	Quadratic sum	Degree of freedom	Mean square value	F ratio	P ratio	Significance
Model	1367.13	14	97.65	66.12	<0.0001	Significant
A-Fly ash particle size	181.28	1	181.28	122.74	<0.0001	***
B-SDS dosage	127.24	1	127.24	86.15	<0.0001	***
C-Ultrasonic time	12.13	1	12.13	8.21	0.0118	*
D-Shaking time	70.11	1	70.11	47.47	<0.0001	***
AB	93.22	1	93.22	63.12	<0.0001	***
AC	84.27	1	84.27	57.06	<0.0001	***
AD	4.80	1	4.80	3.25	0.0917	⊙
BC	7.95	1	7.95	5.38	0.0348	*
BD	25.91	1	25.91	17.54	0.0008	**
CD	104.14	1	104.14	70.51	<0.0001	***
A^2	246.79	1	246.79	167.10	<0.0001	***
B^2	100.94	1	100.94	68.34	<0.0001	***
C^2	61.47	1	61.47	41.62	<0.0001	***
D^2	454.82	1	454.82	307.96	<0.0001	***
Residual error	22.15	15	1.48			
Lack of fit	12.92	10	1.29	0.7001	0.7053	⊙
Pure error	9.23	5	1.85			
Total dispersion	1389.28	29				

3.2.1.2 MV removal rate analysis. For MSAM materials, it was found that there was a significant synergistic effect between alkali–cement ratio, ultrasonic time, hydrothermal time and hydrothermal temperature. According to Fig. 5(a), the interaction between alkali–ash ratio and ultrasonic time was significant ($P = 0.0009 < 0.05$). The removal rate of MV increased first and then decreased with the increase of two factors. The increase of alkali–ash ratio increased the removal rate of MV at the beginning. The extension of ultrasonic time is helpful to improve the removal rate of MV to a certain extent. From

Fig. 5(b), it can be seen that the interaction between alkali–ash ratio and hydrothermal time is extremely significant ($P < 0.0001$). With the increase of alkali–ash ratio and the extension of hydrothermal treatment time, the removal efficiency of MV by MSAM showed a trend of increasing first and then decreasing. The extension of hydrothermal treatment time provides more time for the crystal growth and pore structure improvement of MSAM materials. It can be seen from Fig. 5(c) that the interaction between alkali–cement ratio and hydrothermal temperature was not significant ($P = 0.0997 < 0.05$). It can be seen from
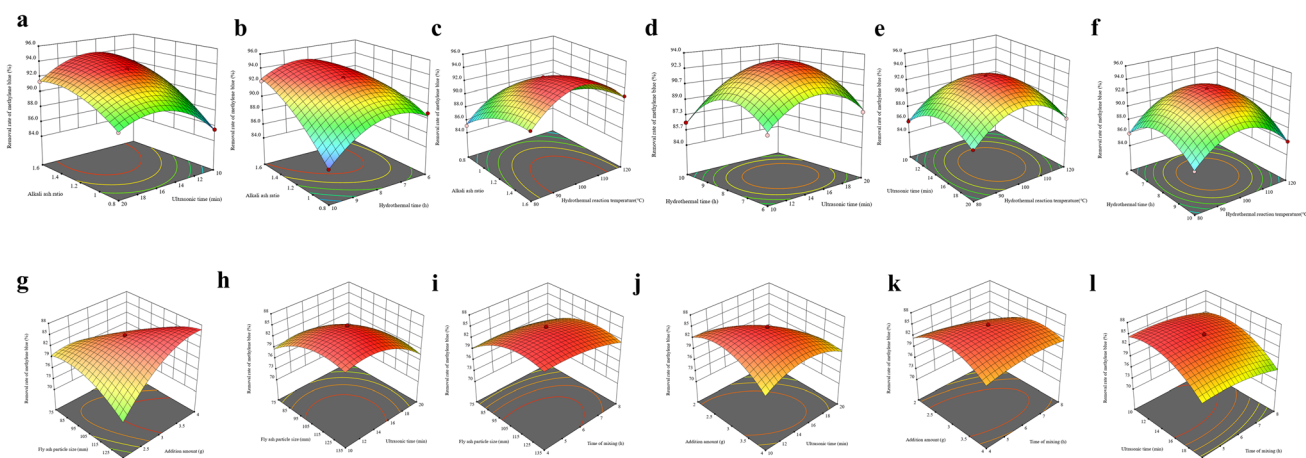

Fig. 4 Response surface plots of MSAM and SDS on MB removal rate under different preparation conditions. (a) Effect of interaction between alkali–ash ratio and ultrasonic time on MB removal rate. (b) Effect of interaction between alkali–ash ratio and hydrothermal time on MB removal rate. (c) Effect of interaction between alkali–ash ratio and hydrothermal temperature on MB removal rate. (d) Effect of interaction between ultrasonic time and hydrothermal time on MB removal rate. (e) Effect of interaction between ultrasonic time and hydrothermal temperature on MB removal rate. (f) Effect of interaction between hydrothermal time and hydrothermal temperature on MB removal rate. (g) The effect of interaction between fly ash particle size and SDS dosage on MB removal rate. (h) The effect of interaction between fly ash particle size and ultrasonic time on MB removal rate. (i) The effect of interaction between fly ash particle size and oscillation time on MB removal rate. (j) The effect of interaction between SDS dosage and ultrasonic time on MB removal rate. (k) The effect of interaction between SDS dosage and oscillation time on MB removal rate. (l) The effect of interaction between ultrasonic time and oscillation time on MB removal rate.
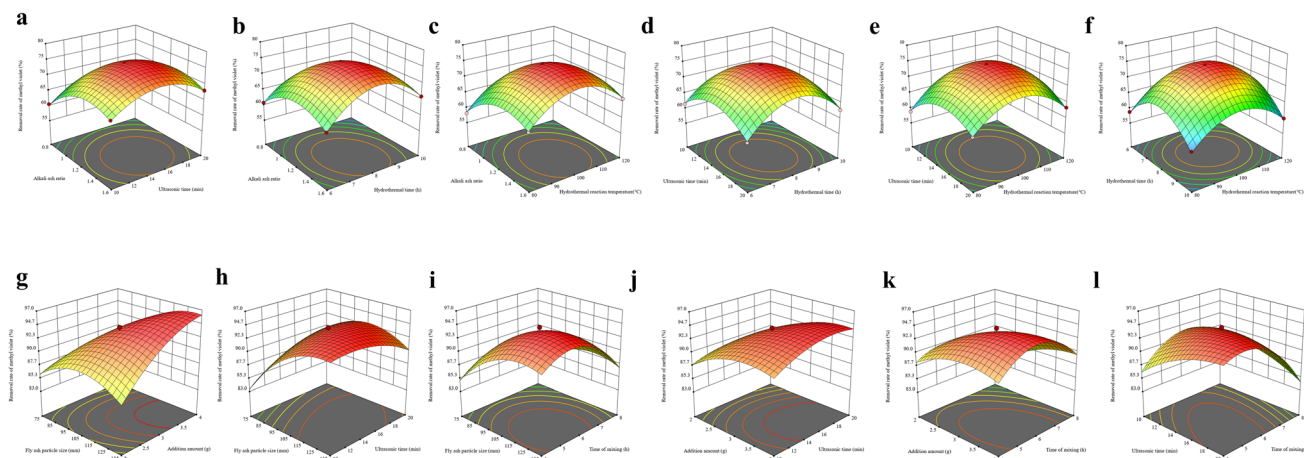
Fig. 5 Response surface plots of MSAM and SDS on MV removal rate under different preparation conditions. (a) Effect of interaction between alkali−ash ratio and ultrasonic time on MV removal rate. (b) Effect of interaction between alkali−ash ratio and hydrothermal time on MV removal rate. (c) Effect of interaction between alkali−ash ratio and hydrothermal temperature on MV removal rate. (d) Effect of interaction between ultrasonic time and hydrothermal time on MV removal rate. (e) Effect of interaction between ultrasonic time and hydrothermal temperature on MV removal rate. (f) Effect of interaction between hydrothermal time and hydrothermal temperature on MV removal rate. (g) The effect of the interaction between fly ash particle size and SDS dosage on the removal rate of MV. (h) The effect of the interaction between fly ash particle size and ultrasonic time on the removal rate of MV. (i) The effect of interaction between fly ash particle size and oscillation time on the removal rate of MV. (j) The effect of interaction between SDS dosage and ultrasonic time on the removal rate of MV. (k) The effect of interaction between SDS dosage and oscillation time on the removal rate of MV. (l) The effect of interaction between ultrasonic time and oscillation time on the removal rate of MV.

Fig. 5(d) that the interaction between ultrasonic time and hydrothermal time was significant ($P = 0.0013$). The MV removal rate increased first and then decreased with the increase of the two factors. Ultrasonic treatment helps to form a more uniform and open pore structure through mechanical vibration and cavitation effects, which is beneficial to the adsorption of dye molecules. It can be seen from Fig. 5(e) that the interaction between ultrasonic time and hydrothermal temperature was extremely significant ($P = 0.0001 < 0.05$). With the increase of hydrothermal temperature and ultrasonic time, the change rule of MV removal rate is consistent. Higher temperatures usually accelerate the chemical reaction, thereby increasing the porosity and specific surface area of the material and providing more adsorption sites for MV molecules. The ultrasonic treatment can disperse the agglomeration structure of fly ash, making the pores of MSAM materials more open, thus improving the adsorption capacity of MV. It can be seen from Fig. 5(f) that the interaction between hydrothermal time and hydrothermal temperature is significant ($P = 0.0084$). Whether the hydrothermal time is prolonged or the hydrothermal temperature is increased, the removal efficiency of MV will increase first and then decrease. Appropriately prolonging the hydrothermal time may be beneficial to the full polymerization of silicon−aluminum compounds and the uniform growth of crystals in MSAM materials. The results showed that the removal rate of MV was up to 89.32% and the adsorption capacity was 17.864 mg g^{-1} under the optimal conditions.

For SDS/FA materials, fly ash particle size (0.25−0.38 mm), SDS dosage (3 g), ultrasonic time (15 min) and oscillation time (8 h) showed a significant synergistic effect. It can be seen from Fig. 5(g) that the interaction between fly ash particle size and

SDS dosage was extremely significant ($P < 0.0001$). With the increase of fly ash particle size and SDS dosage, the removal rate of MV increased first and then decreased. From Fig. 5(h), it can be seen that the interaction between fly ash particle size and ultrasonic time is extremely significant ($P < 0.0001$). With the increase of fly ash particle size and ultrasonic time, the increase of MV removal rate gradually decreases. This is because the smaller particle size of fly ash has a larger specific surface area, which provides more adsorption sites for MV molecules, thereby improving the removal efficiency. From Fig. 5(i), it can be seen that the interaction between fly ash particle size and oscillation time is significant ($P = 0.0917 < 0.05$). The change trend of MV removal rate by fly ash particle size and oscillation time is the same, both of which increase first and then decrease. Appropriate oscillation time can increase the contact opportunity between fly ash and SDS molecules and improve the adsorption efficiency. It can be seen from Fig. 5(j) that the interaction between SDS dosage and ultrasonic time was significant ($P = 0.0348 < 0.05$). When the dosage of SDS is constant, the removal rate of MV increases first and then decreases with the extension of ultrasonic time. This is due to the destruction of the structure of fly ash particles caused by the excessive treatment of ultrasonic waves, which reduces the effective adsorption sites. It can be seen from Fig. 5(k) that the interaction between SDS dosage and oscillation time was significant ($P = 0.0008 < 0.05$). The contour line is more densely distributed on the side of the oscillation time factor, indicating that the oscillation time is dominant in the interaction process of the two factors on the response value. It can be seen from Fig. 5(l) that the interaction between ultrasonic time and oscillation time was extremely significant ($P < 0.0001$). With the

extension of ultrasonic time and oscillation time, the removal rate of MV increased first and then decreased. The results showed that the removal rate of MV was up to 95.38% and the adsorption capacity was 19.076 mg g^{-1} under the optimal conditions.

3.3. Comparative analysis of MSAM and SDS/FA with existing adsorbents

As shown in Table 10, MSAM and SDS/FA exhibit good adsorption performance at pH = 9 compared with other adsorbents, indicating that they are particularly suitable for the treatment of alkaline dye wastewater environment. The data in the table are the performance indicators obtained under the best conditions reported by each.

3.4. Research and analysis of leaching toxicity test

The leachate toxicity of high silicon fly ash (HSFA), MSAM, and SDS/FA was investigated to evaluate the safety of these adsorbents in water treatment. The content of heavy metals in the leachate was measured using a flame atomic absorption spectrophotometer, according to the Chinese national standards GB 5085.3-2007 and HJ/T299-2007. The concentrations of major heavy metals (Cr, Pb, Cu, Cd, Zn, Ni) in the leachates of fly ash, MSAM, and SDS/FA are shown in Table 11. It can be seen from the table that the leaching concentrations of fly ash, MSAM and SDS/FA at pH = 3.2 were lower than the limit value of leaching toxicity (GB 5085.3-2007), and were much lower than the leaching concentration of fly ash at pH = 7.0 and 9.0, indicating that MSAM and SDS/FA had extremely high environmental safety in a wider range of environmental pH (especially under neutral and alkaline conditions), which provided a solid safety basis for the application of adsorbents in actual wastewater treatment.

3.5. Analysis of cyclic regeneration test

The regeneration and reusability performance of MSAM and SDS/FA were further investigated through desorption regeneration experiments to assess the practical and economic

feasibility of these adsorbents in wastewater treatment. As shown in Fig. 6, with the increase in the number of cycles, the removal efficiency of each dye ion gradually decreased to varying extents, indicating that some loss of reduced substances likely occurred during the regeneration process, resulting in a decrease in the content and adsorption sites of MSAM and SDS/FA. After three adsorption–desorption cycles, the removal efficiency of MB and MV by MSAM was 93.87%, 75.26%, and 63.69%, and 89.32%, 72.13%, and 49.1%, respectively. For SDS/FA, the removal efficiency for MB and MV was 83.46%, 75.26%, and 53.69%, and 95.38%, 86.13%, and 76.1%, respectively. These results demonstrate that both MSAM and SDS/FA exhibit good regeneration performance.

3.6. Analysis of characterization results

Through systematic characterization analysis, the significant differences in structural characteristics between MSAM and SDS/FA modified materials and their effects on adsorption performance were revealed.

For MSAM materials, it can be seen from Fig. 7(a) that the surface of fly ash is composed of many fine particles. These smooth spherical particles are due to the presence of more Si–Al matrix components. The structure is relatively dense and there is basically no pore structure (Fig. 7(b)). The surface becomes rough, the structure is loose, the crystal form is obvious, and the pore structure is formed between the grains. The main reason is that under the corrosion of alkali solution, voids and holes appear on the surface, and the alkali fusion residue after ultrasonic treatment further enriches the product. In the hydrothermal reactor, the glass phase in the fly ash is destroyed, so the surface is rougher, showing a block porous structure. From the X-ray diffraction pattern of fly ash in Fig. 7(d), it can be seen that the crystal phase in fly ash mainly includes quartz and mullite, while the amorphous phase is mainly amorphous silicate glass. This structure makes fly ash have certain chemical stability, but also limits its activity in some chemical reactions. The bulge-like broad peak in the figure indicates that the amorphous glass phase in the fly ash is mainly amorphous SiO_2, which may cause the surface of the material to become rougher

Table 10   Comparison of properties of MASM, SDS/FA, and other adsorbents

| Absorbent | q_{m} (mg g^{-1}) | | pH | Dosage (g L^{-1}) | Reference |
	MB	MV			
MASM	115.34	67.20	9	2	This study
SDS/FA	85.49	95.33	9	2	
ZSM-5 zeolite	5.422		11	1.6	43
Denatured fly ash	28.65		7	0.5	44
MS-CFA	10.86		9	0.5	45
Magnetic zeolites	27.05		7	6.25	46
Olive stones	44.5		9	2.8	47
Clay/starch/iron oxide composite		29.67	9	1.5	48
Halloysite nanoclay (HNC)		27.7	4.26	0.4	49
Raw date seeds		59.5	6.5	5	50
Cystoseira tamariscifolia		10	6	7	51
Synthesis of alginate-based composites		57.4	6.5	0.4	52

Table 11 Contents of main heavy metals in HSFA, MSAM, and SDS/FA leachate (mg L^{-1})

Element	PH = 3.2			PH = 7			PH = 9			Leaching toxicity standard value
	HSFA	MSAM	SDS/FA	HSFA	MSAM	SDS/FA	HSFA	MSAM	SDS/FA	
Cr	0.683	0.335	0.429	0.645	0.452	0.317	0.322	0.256	0.183	15
Pb	0.645	0.159	0.176	0.324	0.102	0.086	0.246	0.071	ND	5
Cu	0.524	0.259	0.272	0.257	0.166	0.127	0.167	ND	ND	100
Cd	0.306	0.148	ND	0.109	0.095	ND	0.076	ND	ND	1
Zn	0.233	0.136	0.106	0.178	0.082	0.056	0.133	0.036	0.026	100
Ni	0.068	ND	ND	0.054	ND	ND	0.029	ND	ND	5

and increase the specific surface area of the material, thereby improving its adsorption capacity and activity.[53] From the FTIR diagram of MSAM in Fig. 7(f), it can be seen that the fly ash treated with sodium hydroxide has undergone significant phase transition and structural reorganization. In this process, the phase of the original mullite and quartz crystals in fly ash changed in a strong alkaline environment, forming amorphous silicon–aluminum compounds. This transformation is due to the reaction of sodium hydroxide with silicon aluminum oxide in fly ash, which promotes the dissolution and repolymerization of the original crystal structure.[54] The broad peaks between $2\theta =$ 21.27° and 32.91° indicate the destruction of the fly ash glass phase (amorphous SiO$_2$), leading to a rougher surface, which is consistent with the SEM observation of the development of a honeycomb-like porous structure (pore size 8–15 nm).[55] As shown in the BET results in Fig. 7(i), the specific surface area increased from 0.86 m^2 g^{-1} to 48.92 m^2 g^{-1} (a 58.88-fold increase), and the pore volume increased from 0.0029 cm^3 g^{-1} to 0.1633 cm^3 g^{-1} (a 50-fold increase). The Type IV adsorption isotherm and H1-type hysteresis loop confirm the presence of a regular mesoporous structure. These structural features provide abundant surface hydroxyl groups and ion exchange sites for dye adsorption.

For SDS/FA materials, it can be seen from Fig. 7(c) that a large number of SDS flake crystal fragments are attached to the surface of fly ash after modification. There are obvious white spots on the surface of the modified fly ash, which are the aggregates of SDS crystal fragments. As shown in Fig. 7(e), the

characteristic peaks of quartz (PDF: #83-2465) appeared at 20.76°, 25.56° and 40.62°, and the characteristic peaks of mullite (PDF: #84-1205) appeared at 25.67° and 50.32°.[56] The relative intensity of the characteristic peaks of mullite and quartz in fly ash after reaction is weakened. This is because the crystal phases such as mullite and quartz have strong acid resistance and are not easy to be dissolved.[57] The characteristic peaks of mullite and quartz in the modified fly ash remained unchanged, indicating that the modification process did not disrupt the crystalline structure of the fly ash.[58] Furthermore, the diffraction peaks of the SDS/FA material showed no new crystal phases, confirming that the modification did not induce new crystallographic structures.[59] From the absorption spectrum of fly ash in Fig. 7(g), it can be seen that 1327.46 cm^{-1},1064.75 cm^{-1} and 459.53 cm^{-1} belong to the characteristic absorption peaks of fly ash, and 3629.69 cm^{-1} belongs to the stretching vibration of Al–OH. 1874.37 cm^{-1} is attributed to the stretching vibration of Si–OH.[60] From the absorption spectra of SDS/FA in Fig. 7(e), the symmetric and asymmetric stretching vibration peaks of –CH$_3$ and –CH$_2$ are at 2918.4 cm^{-1} and 2850.33 cm^{-1}, respectively, which belong to the alkyl characteristic peaks of SDS.[61] At 684.19 cm^{-1}, both materials exhibit absorption peaks, indicating the presence of free and associated –OH groups in both.[62] As shown in Fig. 7(j), the specific surface area of SDS/FA (93.59 m^2 g^{-1}) is much higher than that of fly ash (0.86 m^2 g^{-1}), representing an increase of 108.83 times. This is due to the formation of new active sites on the fly ash surface with SDS loading, which is
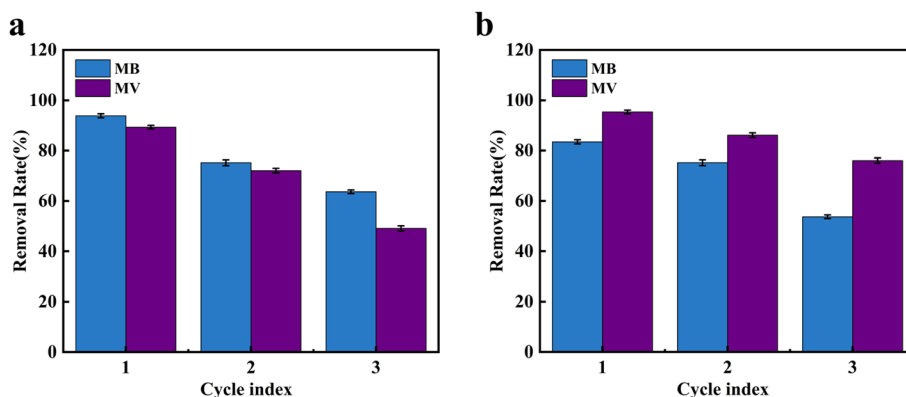

Fig. 6 Cyclic regeneration of MB and MV adsorbed by MSAM and SDS/FA. (a) Cyclic regeneration of MB and MV adsorbed by MSAM. (b) Cyclic regeneration of MB and MV adsorbed by SDS/FA.
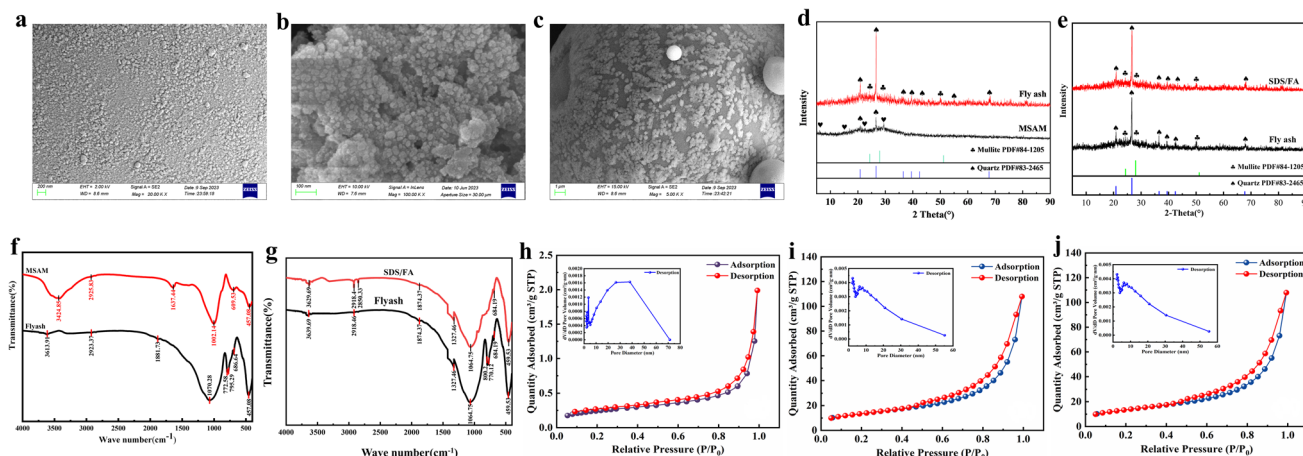
Fig. 7 SEM, XRD, FTIR, and BET characterization of MSAM and SDS/FA. (a) SEM of fly ash. (b) SEM of MSAM. (c) SEM of SDS/FA. (d) XRD of fly ash and MSAM. (e) XRD of fly ash and SDS/FA. (f) FTIR of fly ash and MSAM. (g) FTIR of fly ash and SDS/FA. (h) BET of fly ash. (i) BET of MSAM. (j) BET of SDS/FA.

consistent with the SEM results showing that the modified surface is embedded with a thick layer of SDS, greatly increasing the surface area.[63] The hydrophobic long chains of SDS form a coating on the fly ash surface, providing additional adsorption sites.[64] Additionally, SDS improves the dispersibility of the fly ash particles, reducing particle aggregation and exposing more surface area, thereby increasing the specific surface area. XRD confirms that the crystalline structure of fly ash (quartz at 20.76° and mullite at 25.67°) is preserved during the modification process, and SEM reveals a uniform SDS nanoflake coating (approximately 100 nm). FTIR shows characteristic peaks at 2918.4 cm^{-1} and 2850.33 cm^{-1}, confirming successful modification with SDS. BET analysis shows that the specific surface area increased from 0.86 m^2 g^{-1} to 93.59 m^2 g^{-1} (108.83-fold), which is attributed to the SDS layer formed on the surface and the improved particle dispersion.

3.7. Dynamic experimental analysis of MB and MV in dye wastewater treated by SDS/FA

3.7.1. Analysis of MB removal rate by SDS/FA.
The removal performance of MB by the fly ash dynamic column (1#) and the SDS-FA dynamic column (2#). As observed in Fig. 8(a), upon a detailed analysis of the MB removal efficiency, the experimental data reveal that SDS/FA exhibited a significantly higher removal efficiency for MB during the initial phase of the dynamic experiment. Throughout the entire test, the average removal efficiency of the SDS/FA dynamic column was as high as 68.91%, which is substantially higher than that of unmodified fly ash, which had an average removal efficiency of 34.50%. Over time, although the removal efficiency of SDS/FA for MB decreased, it remained at a relatively high level, stabilizing at 31.10%. This result sharply contrasts with unmodified fly ash, where the removal efficiency dropped from an initial 89.63% to just 5.40% after 28 days. This high and stable performance of SDS/FA can be attributed to its unique modification mechanism. By introducing sodium dodecyl sulfate (SDS), the surface

properties of the fly ash were significantly altered, increasing its hydrophobicity and thus enhancing its adsorption affinity for the hydrophobic organic dye MB. The interaction between the hydrophobic chains of SDS molecules and the MB molecules, along with the electrostatic attraction between the sulfate head groups of SDS and the cationic MB molecules, collectively facilitated the efficient adsorption of MB. Over time, some MB molecules aggregated on the surface of SDS/FA, leading to a decline in the removal efficiency. However, SDS-FA still exhibited superior long-term application potential compared to unmodified fly ash, indicating that chemical modification can significantly improve the adsorption performance of fly ash, especially in treating dye wastewater containing hydrophobic organic dyes. Moreover, the active sites on the SDS/FA surface, along with the π–π stacking interactions and electrostatic interactions with MB molecules, enhanced the adsorption of MB molecules.[65] Additionally, SDS-FA provided more adsorption sites for MB molecules, thereby increasing the adsorption capacity.

3.7.2. Analysis of MV removal rate by SDS/FA.
The removal efficiency of MV by the fly ash dynamic column (3#) and the SDS/FA dynamic column (4#). As observed in Fig. 8(b), both dynamic columns exhibited good removal performance for MV in the early stages of the experiment. SDS/FA demonstrated a high removal efficiency for methyl violet (MV) throughout the entire testing period (28 days), with an average removal efficiency of 65.78%, compared to 27.86% for the fly ash column. Although the removal efficiency of SDS/FA decreased over time, it stabilized at 33.32% by the end of the 28-day test. In contrast, the removal efficiency of fly ash decreased significantly, from 73.48% to 10.30%. The high removal efficiency of SDS/FA for MV is likely attributed to the chemical properties of its modified surface. The introduction of SDS enhanced the electrostatic adsorption of MV molecules, while the pore structure of SDS/FA provided abundant adsorption sites for MV molecules. Over time, the adsorption of MV molecules on the SDS/FA surface gradually reached saturation, which contributed to the decrease
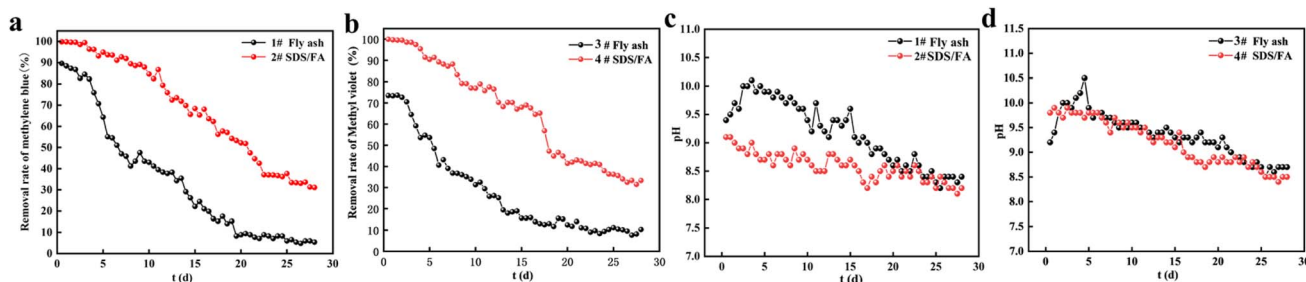
Fig. 8 MB and MV removal rate and dynamic column pH change diagram. (a) The MB removal rate dynamically changes in the dynamic column. (b) The MV removal rate change of the dynamic column. (c) The MB dynamic column pH change diagram. (d) MV dynamic column pH change diagram.

in removal efficiency. Additionally, the hydrophobic groups on the surface of SDS/FA interact with MV molecules through hydrophobic forces, further promoting the adsorption and fixation of MV molecules.[66]

3.7.3. pH change. The pH changes during the treatment of MB wastewater by the fly ash dynamic column (1#) and the SDS/FA dynamic column (2#). As indicated in Fig. 8(c), the pH value of the 1# column initially increased to approximately 10.0 during the first 5 days, primarily due to the reaction of alkaline oxides, such as CaO and MgO, in fly ash with water to form hydroxides. Additionally, the amino and hydroxyl groups of MB molecules formed coordination complexes with the Si–OH groups on the fly ash surface, further promoting the increase in pH. During the mid-phase (5–14 days), the pH gradually decreased, indicating a reduction in the alkaline components of the fly ash. This decrease was accompanied by a decline in the adsorption capacity of the fly ash, increasing the dissociation products of MB, with the released azo groups causing a reduction in pH due to their acidity.[67] In the later phase (14–28 days), the pH of the fly ash column decreased to 8.4, reflecting the depletion of alkaline components in the fly ash and a weakening of its adsorption capacity for MB, leading to the accumulation of acidic dissociation products from MB and a further decrease in pH.

In the 2# column (SDS/FA), during the initial stage (0–2 days), the pH dropped to 8.8, primarily due to the interaction of the sulfate head groups of SDS molecules with the cations in MB and the alkaline substances in fly ash. Between 3 and 28 days, the pH fluctuated between 8 and 9, gradually approaching neutrality, indicating interactions between the basic functional groups of SDS molecules and MB.[68] Compared to the 1# column, the acidic sulfate head groups in SDS/FA caused a further decrease in pH.[69] Although the adsorption capacity of SDS/FA continued to decrease, its pH remained within a relatively stable range.

The pH changes during the treatment of MV wastewater by the fly ash dynamic column (3#) and SDS/FA dynamic column (4#) are shown in Fig. 8(d). In the 3# fly ash column, the pH initially increased to 10.5, as a result of the reaction between the alkaline oxides in fly ash and water, releasing OH− ions and raising the solution's pH. In the later stages, as the alkaline components were consumed and methyl violet (MV)

dissociated, acidic substances gradually accumulated, leading to a gradual decrease in pH, which eventually stabilized at 8.7.

For the 4# SDS/FA column, the pH exhibited a general downward trend, eventually decreasing to 8.5. This decrease was caused by the interaction of the sulfate head groups of SDS molecules with cations in the solution, forming complexes. As cations were adsorbed, the concentration of H+ ions in the solution increased, and the stable adsorption layer formed by SDS/FA adsorption slowed the change in pH, resulting in a more gradual decrease.

4 Conclusion

In view of the problems of accumulation and storage, low comprehensive utilization rate, lack of high-value utilization technology, environmental risk and ecological impact of solid waste fly ash. In this study, two different technical paths were developed in parallel-the preparation of MSAM by alkali fusion–hydrothermal method and the preparation of SDS/FA by surfactant modification method. The optimal preparation conditions were determined by single factor experiment and response surface experiment. The optimal preparation conditions were determined through both single-factor and response surface experiments. Dynamic column experiments were conducted to investigate the removal efficiency of SDS/FA for methylene blue (MB) and methyl violet (MV) in dye wastewater, as well as to analyze its effect on wastewater pH regulation. The specific conclusions are as follows:

The optimal preparation conditions for MSAM were an alkali-to-fly ash ratio of 1.2 : 1, an ultrasonic time of 20 min, a hydrothermal time of 8 hours, and a hydrothermal temperature of 100 °C. Validation experiments showed removal rates of 93.87% for MB and 89.32% for MV. The predicted values from the model deviated by less than 10% from the experimental values, indicating the model can accurately simulate the effects of various factors on the removal rates of MB and MV, thus demonstrating practical value.

The optimal preparation conditions for SDS/FA were a fly ash particle size of 0.18–0.25 mm, SDS dosage of 4 g, ultrasonic time of 20 min, and oscillation time of 8 hours. Under these conditions, removal rates of 83.46% for MB and 95.38% for MV were

obtained. The model predictions were within 10% of the actual results, confirming its accuracy and utility.

Dynamic column tests showed that, after 28 days of operation, the average removal rates of MB and MV in columns 1# and 3# were 34.50% and 27.86%, with effluent pH dropping from 9.4 and 9.2 to 8.4 and 8.7, respectively. In columns 2# and 4# containing SDS/FA, the average removal rates for MB and MV reached 68.91% and 65.78%, with pH declining from 9.1 and 9.8 to 8.2 and 8.5. These findings indicate that SDS modification significantly improves the performance of SDS/FA in the remediation of MB and MV dye wastewater.

Author contributions

Xuying Guo: Conceptualization, Methodology, Validation, Formal analysis, Writing—original draft preparation. Xiaoyue Zhang: Software, Resources, Data curation, Visualization, Writing—review and editing. Xinle Gao: Resources, Project administration, Supervision. Yanrong Dong: Project administration, Supervision, Validation. Zilong Zhao: Investigation, Project administration, Supervision. Honglei Fu: Investigation, Writing—original draft preparation.

Conflicts of interest

The authors declare that they have no known competing financial interests or personal relationships that could have appeared to influence the work reported in this paper.

Data availability

Data will be made available on request.

Acknowledgements

References

1 D. Dong, M. Wu, Y. Yang, Y. Jiao, B. Wang, M. Shao and X. Zhao, *ChemistrySelect*, 2025, **10**, e05659.

2 C. R. Holkar, A. J. Jadhav, D. V. Pinjari, N. M. Mahamuni and A. B. Pandit, *J. Environ. Manage.*, 2016, **182**, 351–366.

3 R. Al-Tohamy, S. S. Ali, F. Li, K. M. Okasha, Y. A.-G. Mahmoud, T. Elsamahy, H. Jiao, Y. Fu and J. Sun, *Ecotoxicol. Environ. Saf.*, 2022, **231**, 113160.

4 M. Guven, B. Isik, F. Cakar and O. Cankurtaran, *Environ. Monit. Assess.*, 2025, **197**, 664.

5 A. Sharma, J. M. Shivanna, N. K. Gupta, P. W. Menezes and G. Hegde, *Chem.–Eur. J.*, 2025, e202501564.

6 S. Chen, Z. Zhao, B. Jiang, Y. Zhang, X. Wang, X. Xu and J. Song, *Materials*, 2025, **18**, 2656.

7 R. Dhanabal and P. G. Priya, *Mater. Sci. Semicond. Process.*, 2025, **192**, 109481.

8 A. S. Hisana, N. Nishat, S. M. Alshehri, T. Ahamad and Z. Haque, *Hybrid Adv.*, 2024, **5**, 100145.

9 J. Fronczyk, K. Kuśmierek and A. Świątkowski, *Water, Air, Soil Pollut.*, 2025, **236**, 138.

10 D. Yanardağ and S. Edebali, *Biomass Convers. Biorefin.*, 2024, **14**, 5699–5710.

11 Z. Chuan, H. Yifen, S. Jingtao, H. Shaohua, M. Minfeng, Z. Liang, L. Kaiwen and G. Yingying, *J. Alloys Compd.*, 2025, **1024**, 180163.

12 M. Gwadera, P. Brzoskwinia, S. Hnatyk and G. Kazberuk, *Purification*, 2025, **1**, 4.

13 U. D. Patil, S. Mahakal, D. M. Nerkar, H. Noothalapati, S. Shinde, S. A. Waghmode and D. Amalnerkar, *Inorg. Chem. Commun.*, 2025, **180**, 114879.

14 M. Visa, M. Cosnita, M. Moldovan, C. A. Marin and M. Mihaly, *Int. J. Environ. Res. Public Health*, 2021, **18**, 3887.

15 Y. Luo, Y. Wu, S. Ma, S. Zheng, Y. Zhang and P. K. Chu, *Environ. Sci. Pollut. Res.*, 2021, **28**, 18727–18740.

16 M. R. Maaze, *Cleaner Mater.*, 2025, **17**, 100329.

17 M. Kuźnia, *Energies*, 2024, **18**, 52.

18 U. B. Deshannavar, B. G. Katageri, M. El-Harbawi, A. Parab and K. Acharya, *Proc. Est. Acad. Sci.*, 2017, **66**, 300.

19 Z. Hussain, N. Chang, J. Sun, S. Xiang, T. Ayaz, H. Zhang and H. Wang, *J. Hazard. Mater.*, 2022, **422**, 126778.

20 Q. Chen, Y. Zhao, Q. Qiu, L. Long, X. Liu, S. Lin and X. Jiang, *Environ. Res.*, 2023, **218**, 114873.

21 Y. Xie, J. Huang, T. Zhao, K. Li, Y. Lu, J. Zhang, C. Li and F. Zhang, *ChemistrySelect*, 2025, **10**, e202406001.

22 S. Dash, H. Chaudhuri, R. Gupta and U. G. Nair, *J. Environ. Chem. Eng.*, 2018, **6**, 5897–5905.

23 M. Fashandi, Z. Ben Rejeb, H. E. Naguib and C. B. Park, *Sep. Purif. Technol.*, 2023, **325**, 124201.

24 R. Jarosz, J. B. Kowalska, K. Gondek, R. Bejger, L. Mielnik, A. H. Lahori and M. Mierzwa-Hersztek, *Agriculture*, 2025, **15**, 786.

25 N. Setthaya, K. Pimraksa, N. Damrongwiriyanupap, D. Panias, P. Mekrattanachai and C. Chindawong, *Chem. Eng. Commun.*, 2023, **210**, 1178–1194.

26 H. Deng, Y. Cheng, J. Li, Q. Zhang, Y. Cao and X. Wang, *Environ. Prog. Sustainable Energy*, 2022, **41**, e13843.

27 C. Krainara, T. Numpilai and T. Witoon, *J. Environ. Chem. Eng.*, 2025, **13**, 118901.

28 M. Davarazar, M. Kamali, C. Venâncio, A. Gabriel, T. M. Aminabhavi and I. Lopes, *Chem. Eng. J.*, 2023, **453**, 139799.

29 W. Wulandari, T. Paramitha, J. Rizkiana and D. Sasongko, *IOP Conf. Ser.: Mater. Sci. Eng.*, 2019, **543**, 012034.

30 Q. Yuan, Y. Zhang, T. Wang, J. Wang and C. E. Romero, *Waste Manag.*, 2021, **135**, 428–436.

31 M. Á. Sanjuán, J. A. Suárez-Navarro, C. Argiz and P. Mora, *J. Radioanal. Nucl. Chem.*, 2020, **325**, 381–390.

32 B. Quintana, M. C. Pedrosa, L. Vázquez-Canelas, R. Santamaría, M. A. Sanjuán and F. Puertas, *Appl. Radiat. Isot.*, 2018, **134**, 470–476.

33 C. Wang, K. Liu, D. Huang, Q. Chen, M. Tu, K. Wu and Z. Shui, *Case Stud. Constr. Mater.*, 2022, **17**, e01422.

34 M. F. Noaman, M. A. Khan, K. Ali and A. Hassan, *Cleaner Mater.*, 2022, **6**, 100151.

35 G. Sheng, S. Zhu, S. Wang and Z. Wang, *RSC Adv.*, 2016, **6**, 26885.

36 V. D. Nguyen, A.-T. Vu and T. V. La, *Particuology*, 2025, **102**, 27–40.

37 A. S. Abdulhameed, A. H. Jawad and A.-T. Mohammad, *Bioresour. Technol.*, 2019, **293**, 122071.

38 I. A. Mohammed, A. H. Jawad, A. S. Abdulhameed and M. S. Mastuli, *Int. J. Biol. Macromol.*, 2020, **161**, 503–513.

39 C. Wang, B. Zhang, X. Sun, Y. Zhang, W. Li, T. Yang, Y. Ma, Z. Sun and T. Li, *Sep. Purif. Technol.*, 2024, **329**, 125140.

40 A. Bavi, M. S. Jafari, M. Heydari, F. Ebrahimi and A. Sadeghizadeh, *Colloids Surf. C Environ. Asp.*, 2023, **1**, 100012.

41 I. M. Imani, N. Noei and S. Azizian, *Colloids Surf., A*, 2020, **587**, 124338.

42 W. Fortas, A. Djelad, M. A. Hasnaoui, M. Sassi and A. Bengueddach, *Mater. Res. Express*, 2018, **5**, 025018.

43 W. Yu, X. Wu, R. Mi, H. Zai, M. Fang, X. Min, Y. Liu and Z. Huang, *J. Am. Ceram. Soc.*, 2024, **107**, 5298–5312.

44 N. T. Dinh, L. N. H. Vo, N. T. T. Tran, T. D. Phan and D. B. Nguyen, *RSC Adv.*, 2021, **11**, 20292–20302.

45 K. Wang, N. Peng, J. Sun, G. Lu, M. Chen, F. Deng, R. Dou, L. Nie and Y. Zhong, *Sci. Total Environ.*, 2020, **729**, 139055.

46 S. Wang, B. Liu, Q. Zhang, Q. Wen, X. Lu, K. Xiao, C. Ekberg and S. Zhang, *J. Cleaner Prod.*, 2023, **390**, 136053.

47 G. Yang, Q. Zhang, Z. Zhao and C. Zhou, *Waste Manag.*, 2023, **156**, 227–235.

48 A. Ansari Mojarad, S. Tamjidi and H. Esmaeili, *Int. J. Environ. Anal. Chem.*, 2022, **102**, 8159–8180.

49 M. Sadiku, T. Selimi, A. Berisha, A. Maloku, V. Mehmeti, V. Thaçi and N. Hasani, *Toxics*, 2022, **10**, 445.

50 N. S. Ali, N. M. Jabbar, S. M. Alardhi, H. S. Majdi and T. M. Albayati, *Heliyon*, 2022, **8**, e10276.

51 M. I. Al-Zaban, N. K. Alharbi, F. M. Albarakaty, S. Alharthi, S. H. A. Hassan and M. A. Fawzy, *Sustainability*, 2022, **14**, 5285.

52 Z. Samuel, M. O. Ojemaye, O. O. Okoh and A. I. Okoh, *Results Chem.*, 2022, **4**, 100579.

53 S. V. Vassilev and C. G. Vassileva, *Fuel*, 2009, **88**, 235–245.

54 J. Dobrzyńska, M. Dąbrowska, R. Olchowski, E. Zięba and R. Dobrowolski, *J. Environ. Chem. Eng.*, 2021, **9**, 105302.

55 V. Gadore and M. Ahmaruzzaman, *J. Water Process Eng.*, 2021, **41**, 101910.

56 A. S. Abdulhameed, A. H. Jawad and A.-T. Mohammad, *Bioresour. Technol.*, 2019, **293**, 122071.

57 I. A. Mohammed, A. H. Jawad, A. S. Abdulhameed and M. S. Mastuli, *Int. J. Biol. Macromol.*, 2020, **161**, 503–513.

58 A. H. Jawad, N. S. A. Mubarak and A. S. Abdulhameed, *Int. J. Biol. Macromol.*, 2020, **142**, 732–741.

59 V.-P. Dinh, M.-D. Nguyen, Q. H. Nguyen, T.-T.-T. Do, T.-T. Luu, A. T. Luu, T. D. Tap, T.-H. Ho, T. P. Phan, T. D. Nguyen and L. V. Tan, *Chemosphere*, 2020, **257**, 127147.

60 V. I. Isaeva, K. E. Papathanasiou and L. M. Kustov, *Crystals*, 2020, **10**, 617.

61 J. Pizarro, X. Castillo, S. Jara, C. Ortiz, P. Navarro, H. Cid, H. Rioseco, D. Barros and N. Belzile, *Fuel*, 2015, **156**, 96–102.

62 L. Ren, D. Zhou, J. Wang, T. Zhang, Y. Peng and G. Chen, *J. Mol. Liq.*, 2020, **309**, 113074.

63 S. Payamifar, M. Abdouss, A. Poursattar Marjani and H. Sarreshtehdar Aslaheh, *J. Organomet. Chem.*, 2025, **1036**, 123687.

64 V.-P. Dinh, N.-C. Le, L. A. Tuyen, N. Q. Hung, V.-D. Nguyen and N.-T. Nguyen, *Mater. Chem. Phys.*, 2018, **207**, 294–302.

65 C. Jin, J. Sun, Y. Chen, Y. Guo, D. Han, R. Wang and C. Zhao, *Sep. Purif. Technol.*, 2021, **276**, 119270.

66 A. H. Jawad and A. S. Abdulhameed, *Surf. Interfaces*, 2020, **18**, 100422.

67 M. Usman, I. Anastopoulos, Y. Hamid and A. Wakeel, *Environ. Sci. Pollut. Res.*, 2022, **30**, 124427–124446.

68 S. Agarwal, P. Rajoria and A. Rani, *J. Environ. Chem. Eng.*, 2018, **6**, 1486–1499.

69 H. Sun, J. Zhan, L. Chen and Y. Zhao, *Appl. Surf. Sci.*, 2023, **607**, 155135.